Supplementary Information

Luminescent lanthanide nanoparticle-based imaging enables ultra-sensitive, quantitative and multiplexed *in vitro* Lateral Flow Immunoassays

F. Mousseau[a*], C. Féraudet Tarisse[b], S. Simon[b], T. Gacoin[c], A. Alexandrou[a†] and C. I. Bouzigues[a†]

[a]: *Laboratoire d'Optique et Biosciences, Ecole Polytechnique, Institut Polytechnique de Paris, CNRS, INSERM, Route de Saclay, 91128 Palaiseau, France.*
[b]: *Université Paris-Saclay, CEA, INRAE, Département Médicaments et Technologies pour la Santé (DMTS), 91191 Gif-sur-Yvette, France.*
[c]: *Laboratoire de Physique de la Matière Condensée, Ecole Polytechnique, Institut Polytechnique de Paris, CNRS, Route de Saclay, 91128 Palaiseau, France.*

Outline

S1 – Chemicals, salts and toxins 2
S2 – Nanoparticle synthesis, functionalization and characterization 3
S3 – Strip preparation 7
S4 – Schematic representation of the LEDs arrangement inside the homemade reader 8
S5 – LFA quantitative analysis of strips labeled with Eu NPs 9
S6 – LFA sensitivity by visual inspection of strips labeled with Au and Eu nanoparticles 10
S7 - Influence of the strip batch on LFA sensitivity 11
S8 – Non-specific adsorption of nanoparticles on the nitrocellulose membrane 12
S9 – Non-linear fit of the calibration curves 13
S10 - Quantitative analysis of strips labeled with gold nanoparticles 14
S11 - Study of the potential cross-talk in view of multiplexing 15
S12 – Quantitative analysis of multiplexed strips labeled with Eu nanoparticles 16
S13 – Multiplexed strips with different toxin concentrations 17
References 18

Corresponding author: fanny.mousseau@polytechnique.edu

S1 – Chemicals, salts and toxins

S1.1 Chemical and salts

Europium (III) nitrate pentahydrate, sodium orthovanadate, succinic anhydride, N-(3-dimethylaminopropyl)-N'-ethylcarbodiimide hydrochloride (EDC), N-hydroxysulfosuccinimide sodium salt (NHS), ethanolamine hydrochloride, sodium azide, glycerol, potassium dihydrogen phosphate (KH_2PO_4), dipotassium hydrogen phosphate (K_2HPO_4), sodium dihydrogen phosphate (NaH_2PO_4), disodium hydrogen phosphate (Na_2HPO_4), sodium chloride (NaCl), Trizma® hydrochloride (Tris-HCl), bovine serum albumin (BSA), MES sodium salt, phosphate buffer saline (PBS) and N-N-dimethylformamide (DMF) were purchased from Sigma Aldrich.
Sodium hydroxide (NaOH, 10 $mol.L^{-1}$), (3-aminopropyl)triethoxysilane (APTES) and D-glucose came from Fisher Chemicals.
Yttrium (III) nitrate hexahydrate, Tween 20 and absolute ethanol were provided by Merck.
Glycine and ethanol (96 v%) were supplied by VWR Chemicals (Prolabo, GPR recapter).
Rhodamine 6G, the protein assay dye reagent concentrate (Bradford) and the Pierce BCA protein assay kit were purchased respectively from ACROS Organics, Biorad and Thermo Scientific.

S1.2 Toxin production

Briefly, the DNA sequences of the *sea*, *seg*, *seh* and *sei* genes were obtained from the publicly available genetic sequence database GenBank and optimized for protein expression in the bacterium *E. Coli*. The optimized DNA sequences were inserted in plasmids, enabling their internalization by the bacteria and the production of the corresponding toxins. After culture of *E. Coli* bacteria to induce their proliferation, toxins were extracted and purified by chromatography. More details are available in our previous work[1].

S2 – Nanoparticle synthesis, functionalization and characterization

1) Synthesis and functionalization of europium-doped nanoparticles

YVO_4:Eu nanoparticles of YVO_4 doped with 40 % of europium were synthesized by aqueous co-precipitation following a protocol adapted from our previous work[2]. Briefly, two aqueous solutions of 25 ml of the precursor salts were freshly prepared. One contained 0.1 M of sodium orthovanadate and the other contained yttrium nitrate at 0.06 M and europium nitrate at 0.04 M in Milli-Q water. The solution of lanthanides was then rapidly added into the solution of vanadate under vigorous stirring. After 5 min, the pH of the solution was adjusted to pH 9 through the addition of 1 N NaOH. After 2 hours of ageing, the solution was centrifuged at 2 630 g for 20 min. The precipitate was then redispersed in pure water and sonicated for 2 min with a 450 W Branson sonifier. These centrifugation/redispersion steps were repeated 3 times to ensure the removal of counter-ions, as attested by a conductivity lower than 100 $\mu S.cm^{-1}$. The final solution, with a volume adjusted to 50 ml, was then centrifuged at 789 g for 5 min to remove possible aggregates. The resulting colloidal suspensions of YVO_4:Eu (40 %) NPs was homogeneous and slightly light diffusing.

Particles were then silicated, aminated and carboxylated according to previous work[3,4] to enable their covalent coupling with antibodies (Figure S2.1). In short, 2.5 mL of sodium silicate were added dropwise to 25 mL of nanoparticles at 20 mM of vanadate. The suspension was stirred over night at room temperature and purified as detailed above. Then, 75 mL of silicated NPs at 3 mM of vanadate were added at 1 $mL.min^{-1}$ using a peristaltic pump to 225 mL of boiling ethanol containing 265 µL of APTES. The reaction solution was further refluxed for 24 hours to ensure the formation of a uniform cross-linked aminated network around the NPs, leading to a covalent shell of amines surrounding the particles. The NPs were purified as described previously but with particle redispersion in an ethanol:water mixture (3:1) instead of pure water. Finally, particles were transferred into DMF and 1 mL of these NPs at 40 mM of vanadate were added to 10 mL of succinic anhydride (0.1 $g.mL^{-1}$ in DMF). The suspension was stirred overnight under inert atmosphere and purified by 3 cycles of centrifugation/dispersion in MES buffer (50 mM, pH 5 to 6).

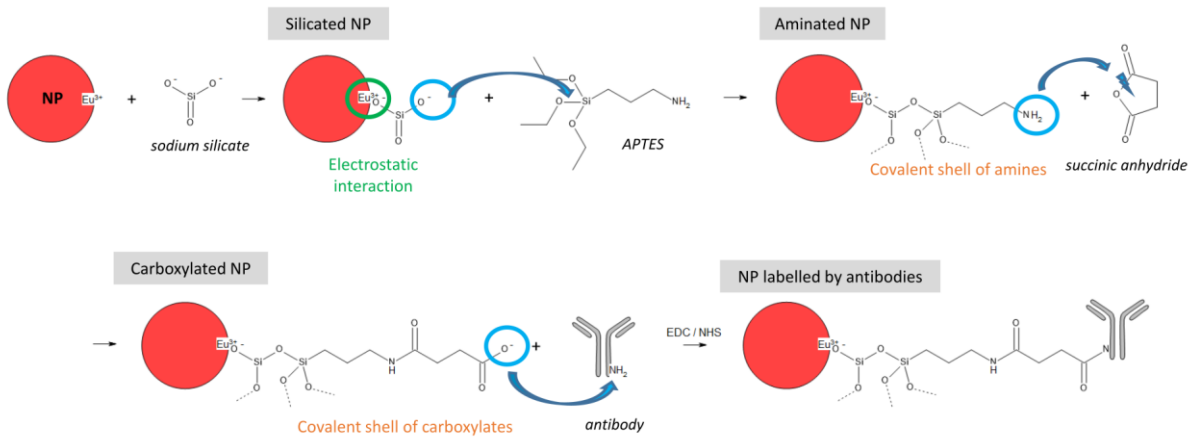

Figure S2.1: Europium-doped nanoparticle functionalization and coupling to detection antibodies.

2) Nanoparticle characterization

Au NPs

Gold NPs (BBI Solutions, EM.GC40, Batch 200 600 92, geometric diameter: 40.8 nm – standard deviation: 8 %) were characterized as received by several techniques. Their hydrodynamic diameter was determined with the Zetasizer Nano ZS equipment (Malvern Instruments, UK). Measurements were performed in triplicate at 25 °C after an equilibration time of 120 s. Nanoparticles exhibited a diameter of 41.4 nm, in agreement with the size determined via transmission electron microscopy by the supplier.

The absorbance of the Au NPs was measured on a UV-1700 pharmaSpec spectrophotometer (Shimadzu), as displayed in Figure S2.2. The surface plasmon resonance peak was observed at 526 nm, which is in agreement with the particle diameter[5]. The Au NPs molar extinction coefficient at 450 nm, ε_{450}, was estimated to be $\varepsilon_{450} = 5.32 \times 10^9\ cm^{-1}.L.mol^{-1}$ from their size[5]. Using the absorbance of the NPs at 450 nm, we determined the Au NP molar concentration to be equal to 0.357 $nmol.L^{-1}$. Assuming 59 atoms per nm^3 of gold nanoparticle, this molar concentration was converted to mass concentration[6], giving a stock solution at 150 $\mu g.mL^{-1}$.

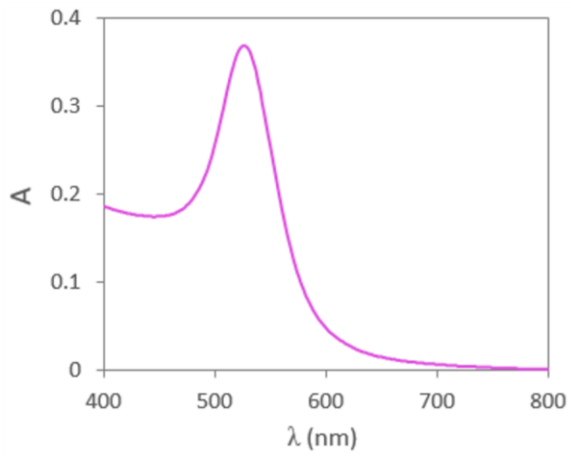

Figure S2.2: Absorbance spectrum of the gold nanoparticles in the visible range (dilution of the stock solution: 1/11 in Milli-Q water).

Eu NPs

The europium-doped NPs were characterized after synthesis and after each functionalization step. Basically, the size distributions, charge and the spectral properties were obtained by dynamic light scattering (DLS) and transmission electron microscopy (TEM), zeta potential measurements, and UV-vis spectroscopy, respectively.

For the TEM measurements, 2 µL of NP solution was deposited on a formvar/carbon-coated 400 mesh copper grid for 3 min. Then the solution in excess was absorbed by a filter paper and the grid was air dried. NPs were observed on a JEOL JEM-1400 microscope operating at 120 kV. Images were acquired with a high-speed camera (SC1000 Orius, Gatan), processed with Digital Micrograph (Gatan) and analysed quantitatively with the ImageJ software. The inset of the Figure S2.3a displays a TEM image of the Eu NPs. It shows that they are oblong and that their contours are not well defined. This is because Eu NPs are a polycrystalline assembly of monocrystalline grains with a low degree of crystallinity[7]. In addition, following the drying inherent in the preparation of the samples, the nanoparticles are aggregated, which makes it difficult to visualize isolated particles. Nevertheless, short and long axis were manually measured for more than 200 nanoparticles giving mean values of 26.3 ± 13.5 nm and 12.0 ± 5.6 nm, the size distribution being displayed in Figure S2.3a and Figure S2.3b, respectively. Knowing that the crystalline cell of the vanadate matrix (7.123 Å x 7.123 Å x 6.291 Å) contains four

$Y_{0.6}VO_4Eu_{0.4}$ units, the parameters determined by TEM lead us to estimate that 1 mM of vanadate corresponds to 22.9 nM of NPs[8].

The hydrodynamic diameter of the nanoparticles, based on the intensity distribution obtained from the dynamics light scattering measurements, were, respectively, 180, 130, 160 and 130 nm for the bare, silicated, aminated and carboxylated nanoparticles. This large diameters are probably due to the relative polydispersity of the nanoparticles and to the fact that DLS measurements, in particular the intensity distribution, strongly overestimate the contribution of larger particle sizes.

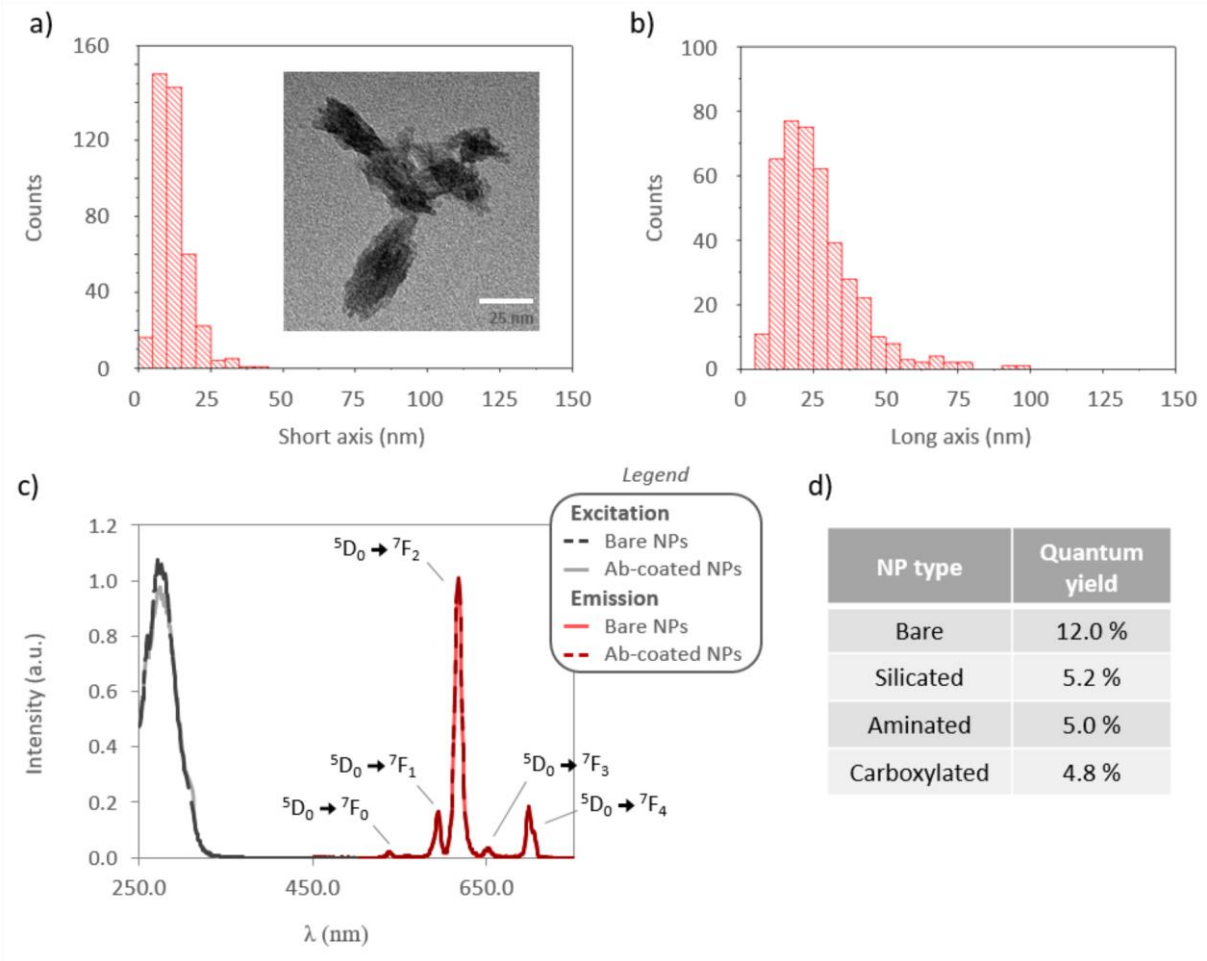

NP type	Quantum yield
Bare	12.0 %
Silicated	5.2 %
Aminated	5.0 %
Carboxylated	4.8 %

Figure S2.3: a, b) Size distribution of the short (a) and long (b) axis of the Eu NPs from TEM images. Inset: example of a TEM image. c) Excitation (grey lines) and emission (red lines) spectra of the europium-doped nanoparticles either bare (dashed lines) or coupled to antibodies (continuous lines). Nanoparticles were diluted in Milli-Q water at 10 µM of vanadate ions. The excitation spectrum was obtained for the emission wavelength of 617 nm while the emission spectrum was obtained by exciting the particles at 280 nm. The signal intensity I was expressed in arbitrary units (a.u.). d) Quantum yield of bare, silicated, aminated and carboxylated nanoparticles. After an initial decrease of the quantum yield upon silica coating, the subsequent functionalization steps did not modify the nanoparticle quantum yield.

The zeta potential was determined with the Zetasizer Nano ZS equipment (Malvern Instruments, UK) for particles at 0.4 mM of vanadate ions. Measurements were performed in triplicate at 25 °C after an equilibration time of 120 s. Bare, silicated, aminated and carboxylated nanoparticles exhibited a zeta potential at +27, -16, +28 and -14, suggesting that the successive functionalization steps ran smoothly. Excitation and emission spectra were recorded on Cary Eclipse Varian fluorometer for nanoparticles at 10 µM of vanadate ions in Milli-Q water, showing that Eu NPs exhibit maximum absorbance and luminescence at 280 nm and 617 nm, respectively (Figure S2.3c).

The quantum yield was determined by the "Relative Determination Method"[9]. Absorption (Shimadzu spectrophotometer) and fluorescence spectra (Fluorolog®, Horiba) were measured for Rhodamine 6G (5 µM) and Eu-doped nanoparticles (10 µM of vanadate) in absolute ethanol and pure water, respectively. The quantum yield Φ was then calculated following the formula of Demas and Crosby:

$$\Phi = \Phi_r . \left(\frac{n_s}{n_r}\right)^2 . \frac{1 - 10^{-A_r}}{1 - 10^{-A_s}} . \frac{I_s}{I_r} . \frac{f_r}{f_s}$$

In this equation, the subscripts s and r denote the sample and the reference, Φ_r is the fluorescence quantum yield of the reference (here 0.95), n is the refractive index of the solvents ($n_s = 1.33$ for water and $n_r = 1.36$ for absolute ethanol), A denotes the absorbance at the excitation wavelength employed for the fluorescence spectra measurement (here 280 nm), I represents the spectrally integrated fluorescence signal and f is the instrumental function. Fixing the same measurement parameters (excitation wavelength, slit width, integration times, spectral range, …) for the sample and the reference ensured $f_s = f_r$. With this protocol, the quantum yield of the nanoparticles was determined for the different surface functionalization (Figure S2.3.d). Results show that bare NPs have a quantum yield of 12 %. Silica coating induces a significant decrease in the quantum yield, which however remains constant at around 5 % after the next surface modification steps.

3) Nanoparticle coupling to antibodies

Detection antibodies were adsorbed on gold nanoparticles according to the following protocol. Briefly, 100 µL of antibodies (250 µg.mL^{-1} in potassium phosphate buffer – 2 mM, pH 7.4) were added to 800 µL of nanoparticles (350 pM) and the solution was stirred in the dark for 1 h. Then, 100 µL of a precipitating solution (1 % of BSA in potassium phosphate buffer – 20 mM, pH 7.4) was added to the suspension prior to purification by 2 cycles of centrifugation (15 min, 15 000 g) and dispersion in a conservation solution (0.1 % of BSA in potassium phosphate buffer - 2 mM, pH 7.4).

Detection antibodies were covalently bound to the Eu-doped nanoparticles. To this aim, the carboxylic functions of the NPs (1 µmol of vanadate ions) were activated by 430 µL of an EDC / NHS mixture (0.5 mg.mL^{-1} of each reactant in MES buffer) during 25 min under stirring. The excess of EDC / NHS was removed by centrifugation and NPs were re-suspended in 125 µL of antibody solution (final concentration: 0.55 mg.mL^{-1} in MES), giving an Ab to NP molar ratio of 20. After 1 h of incubation at 37 °C under stirring, the particles were transferred to a blocking buffer (2 % of BSA and 100 mM of ethanolamine hydrochloride in PBS) for 1 h of passivation, then purified by alternating centrifugation and dispersion in a conservation buffer (0.05 % of Tween20, 0.1 % of glycine and 10 % of glycerol in potassium phosphate buffer – 10 mM, pH 7.4). Note that the coupling ratio was verified before the passivation step with a Bradford assay performed on the supernatant and a BCA assay carried out on the nanoparticle pellet. A coupling efficiency close to 100% was obtained.

Excitation and emission spectra of the coupled nanoparticles were recorded as described above and displayed in Figure S2.3.c. The spectra of bare and antibody-conjugated nanoparticles are superimposable. Considering in addition that the quantum yield of the nanoparticles seems affected only by the first step of their surface modification (as discussed previously), we may assume that the excitation and emission spectra of the coupled NPs as well as their quantum yield will not be modified in more complex environments like in sample matrices or in LFA strips.

S3 – Strip preparation

S3.1 –Treatment, assembly, cutting and conservation of strips

After antibody deposition on the nitrocellulose, membranes were treated to limit non-specific signals, surface corrosion or antibody denaturation induced by the complex interactions arising between the inorganic reporters, the nitrocellulose and the antibodies[10]. Briefly, membranes were dried at 37 °C for 20 min, immersed 30 min in a saturation solution (0.5 % BSA and 150 mM NaCl in sodium phosphate buffer - 10 mM, pH 7.4), rinsed with Milli-Q water, incubated 20 min in a conservation solution (0.1 % Tween 20 and 7.5 % glucose in sodium phosphate buffer - 10 mM, pH 7.4) and dried at 37 °C for 20 min. Subsequently, an absorption pad (SureWick CFSP 203000, Merck) and a conjugate pad (Glass Fiber Diagnostic Pad GFDX 083000, Merck) were attached, overlapping the nitrocellulose membrane on 2 mm. This assembled membrane card was hand-rolled to ensure adhesion of the different components and was then cut into 5 mm wide strips using a CM5000™ Guillotine Cutter (BioDot, USA). The prepared strips were then stored with desiccant at room temperature before use.

S3.2 - Influence of the test line position on LFA sensitivity for multiplex strip preparation

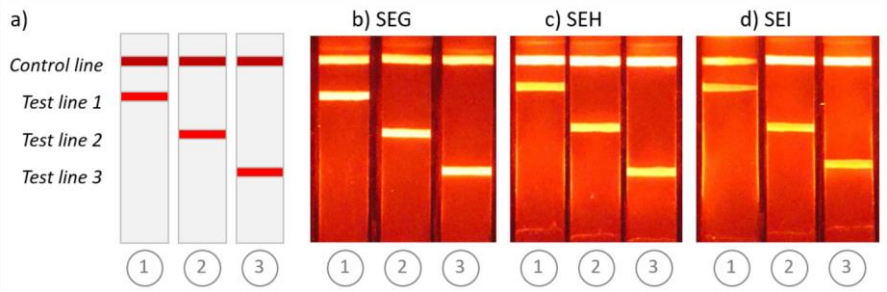

Figure S3.1: a) Representation of the strips designed to study the influence of the test line position on the assay sensitivity. b-d) Assays performed with the toxins SEG (b), SEH (c), and SEI (d) at 1 ng.mL^{-1} using Eu NP probes.

S3.3 – Performing an LFA assay in a dipstick format

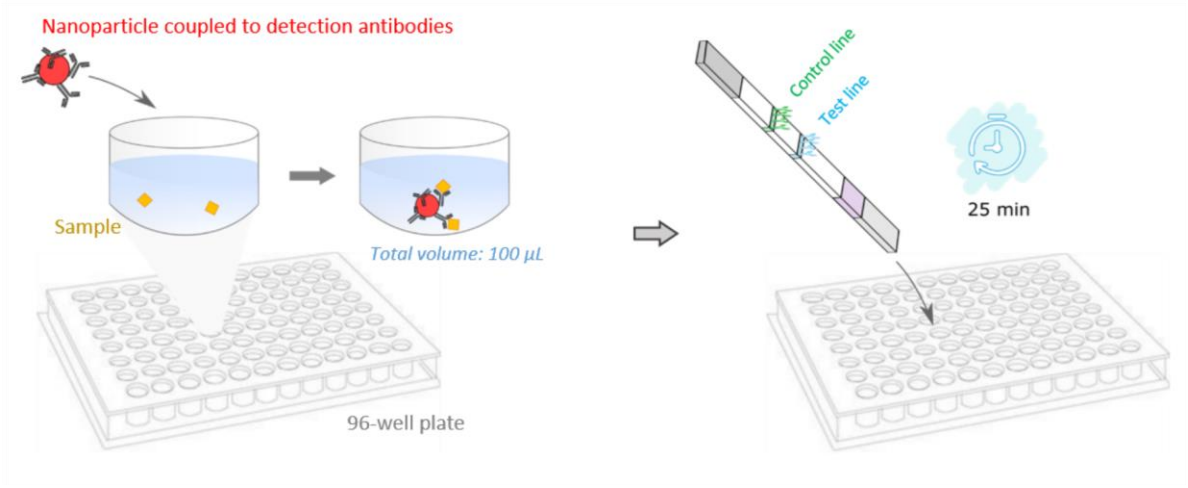

Figure S3.2: Schematic representation of how we perform LFA assays in the dipstick format.

S4 – Schematic representation of the LEDs arrangement inside the homemade reader

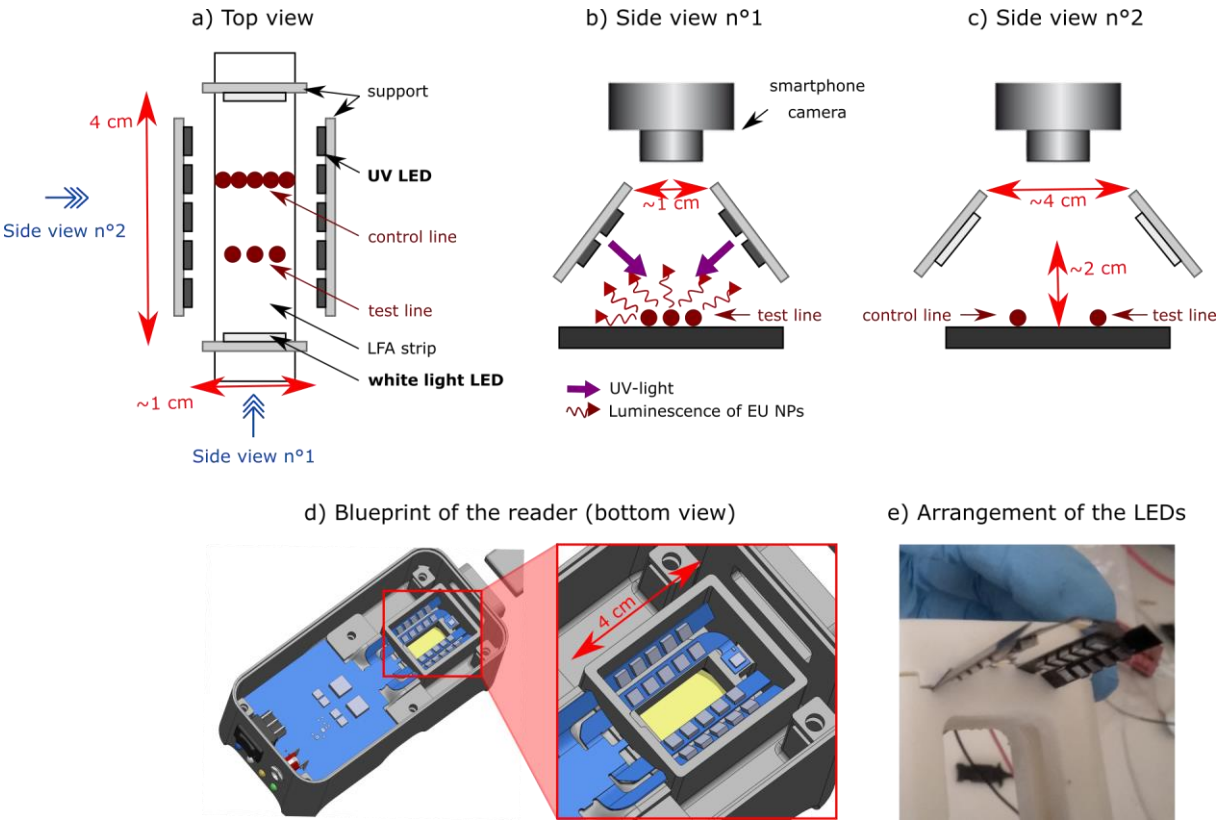

Figure S4: a) Top view of the arrangement of UV LEDs and white light LEDs above the LFA strip. The camera has been removed from this scheme for clarity. b) Side view n°1. The white light LEDs, which are in the foreground and in the background, have not been shown to simplify the visualization of the assembly. c) Side view n°2. The UV LEDs, which are foreground and background in this view, are not displayed to help to visualize the system. d) Blueprint displaying a bottom view of the reader (BitMaker, Paris). The inset shows the 20 UV LEDs (2 mW LEUVK37B50HF00, Laser Components) and the 2 white light LEDs. e) Picture of the arrangement of the LEDs leading to a typical excitation intensity of ~ 4 mW/cm^2.

S5 – LFA quantitative analysis of strips labeled with Eu NPs

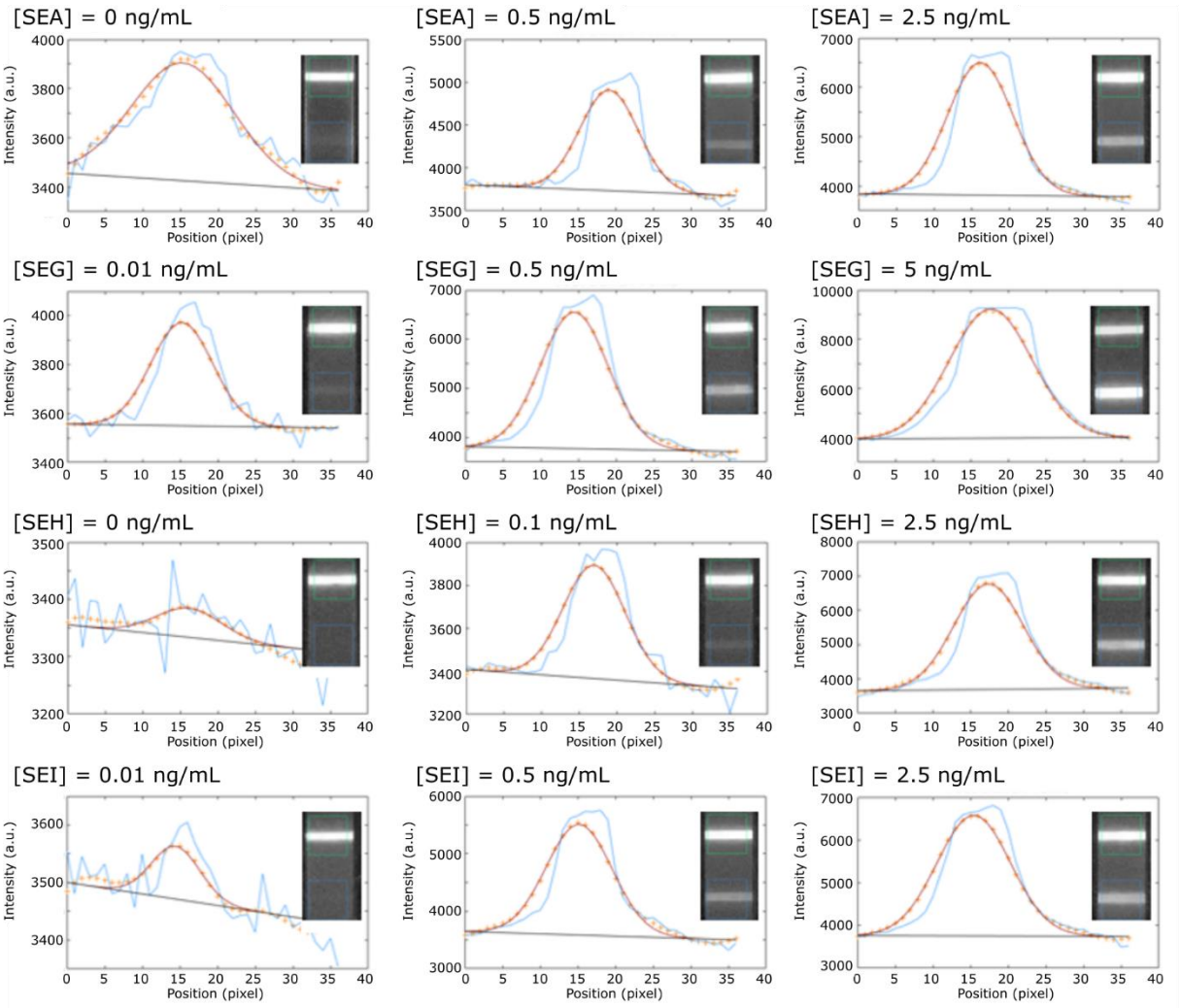

Figure S5: Examples of LFA quantitative analysis for strips labeled with Eu NPs. The raw data are in blue, the curves after convolution by a Gaussian function are in orange. The Gaussian fits of the convoluted data and the background are respectively in red and grey. Note that the ordinate scale varies from one graph to another, thus making it possible to show that the data analysis is suitable regardless of the amplitude of the peak and the associated noise. Insets show strips with green and blue rectangles indicating the ROI localization around the control and test lines, respectively.

S6 – LFA sensitivity by visual inspection of strips labeled with Au and Eu nanoparticles

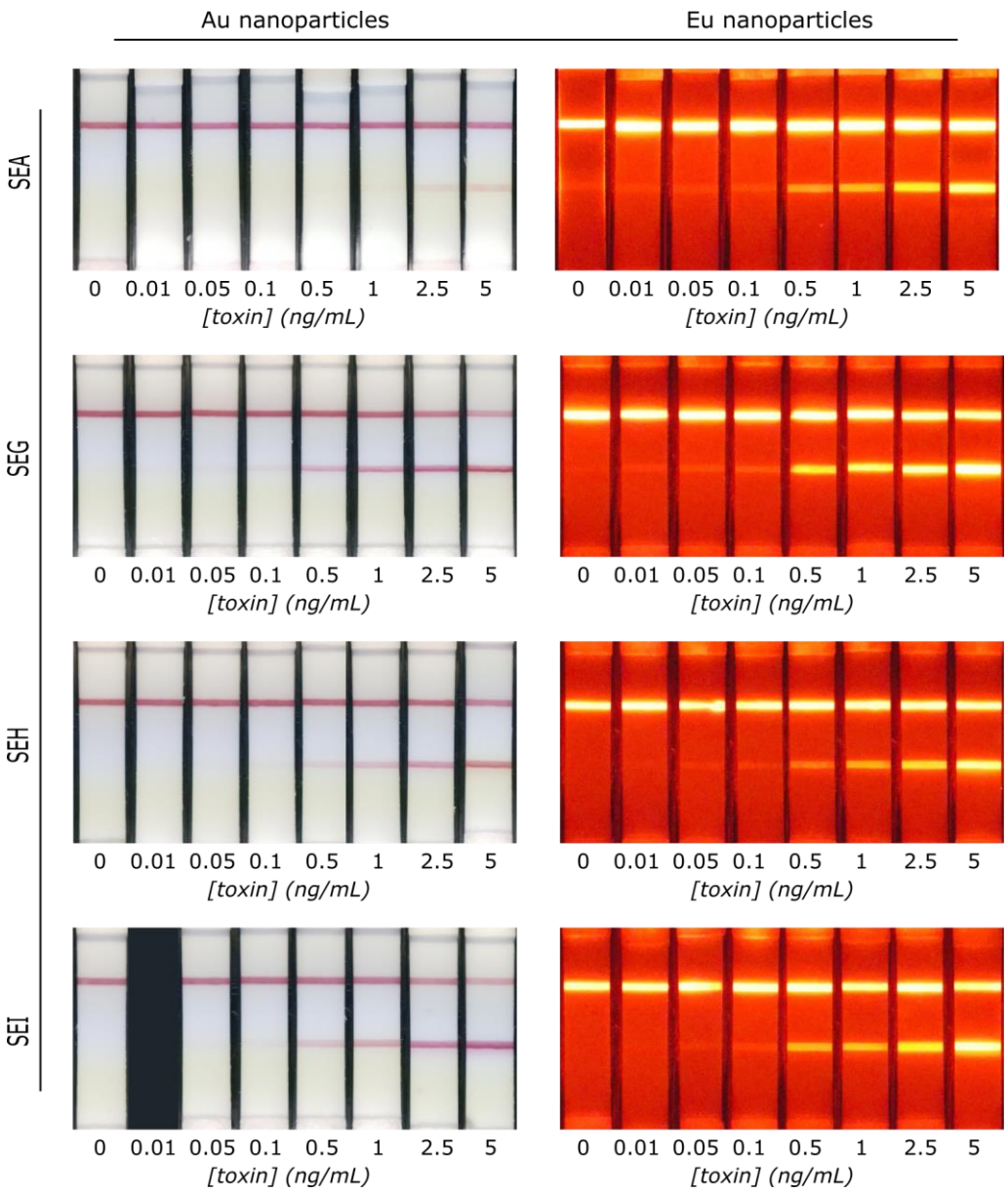

Figure S6: LFA strips labeled with gold and europium-doped nanoparticles for the detection of the SEA, SEG, SEH, and SEI toxins (concentrations ranging from 0.01 to 5 ng.mL^{-1}).

NPs	Sensitivity (ng.mL^{-1})			
	SEA	SEG	SEH	SEI
Au	2.5	0.1	0.5	0.5
Eu	0.5	0.01	0.05	0.05
Gain	**5**	**10**	**10**	**10**

Table S6: Approximate lowest detectable concentrations and sensitivity gains obtained by visual inspection of the strips labeled with Au and Eu NPs.

S7 - Influence of the strip batch on LFA sensitivity

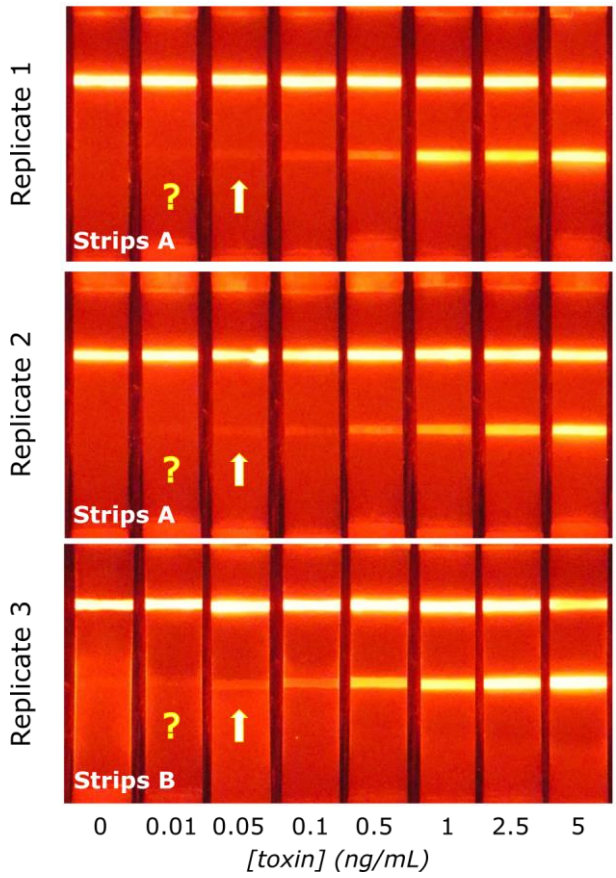

Figure S7: LFA strips labeled with europium-doped nanoparticles for the detection of SEH (from 0.01 to 5 ng.mL^{-1}). The first two replicates are made with a first batch of strips (strips A), the third one with a second batch (strips B) made from the same batches of nitrocellulose membrane, sample pad, absorption pad and antibodies. The difference between the two strip batches is the day of the strip preparation.

S8 – Non-specific adsorption of nanoparticles on the nitrocellulose membrane

LFA were performed in the absence or presence of europium-doped nanoparticles. The mean value of the intensity of the R, G, and B channels of the pictures were measured on the strip – including autofluorescence and non-specifically adsorbed nanoparticles - and on the strip holder in the Regions Of Interest (ROIs) shown in Figure S8. The final signal, defined as the difference between intensities coming from the strip and the holder, was typically 2 times higher in the presence of the Eu NPs. These results indicated that a significant part of the background was not due to the autofluorescence of the strip but rather to the non-specific adsorption of nanoparticles all along the strip during migration. This showed that, in our acquisition regime, autofluorescence did not prevent from reliably detecting the lowest nanoparticle concentrations deposited on the strip. This phenomenon was not limited to our luminescent particles: by imaging fully dried strips (1 days) labelled with gold NPs, non-specific adsorption was also observed (data not shown).

The sensitivity was thus not limited by the minimal number of detectable probes but by the residual signal coming from the non-specific adsorption of NP-Ab conjugates along the strip.

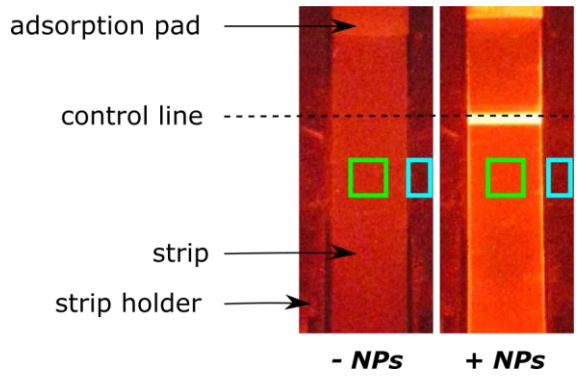

Figure S8: Typical LFA performed without toxin in the presence or absence of Eu NPs for the same nanoparticle concentration as the one used in the toxin experiments. Intensities were measured via ImageJ in the green and blue Regions Of Interest (ROIs) respectively placed on the strip and strip holder. The values were respectively 87 and 59 for the strip and its holder in the absence of NPs, and 104 and 59 in the presence of the latter, giving final signals of respectively 28 and 45 in the absence and presence of particles.

S9 – Non-linear fit of the calibration curves

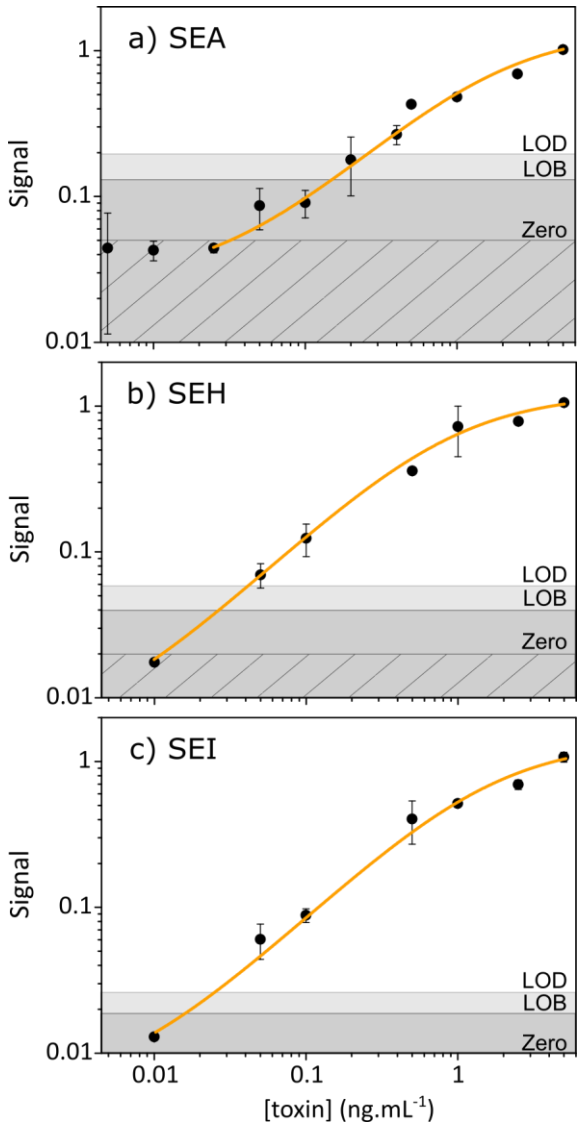

Figure S9: Quantitative analysis of range of SEA (a), SEH (b), and SEI (c) concentrations obtained in independent duplicates with Eu-doped NPs as probes (error bars indicate the standard deviation of two independent replicates). The experimental data are fitted (orange curves) by Signal = A.[toxin] / (B + [toxin]) + C. The obtained constants A, B, C, and the fit residuals respectively equal 1.29, 1.79, 0.02, and 0.98 for SEA, 1.18, 0.89, 0.005, and 0.99 for SEH, and 1.32, 1.58, 0.005, and 0.99 for SEI.

S10 - Quantitative analysis of strips labeled with gold nanoparticles

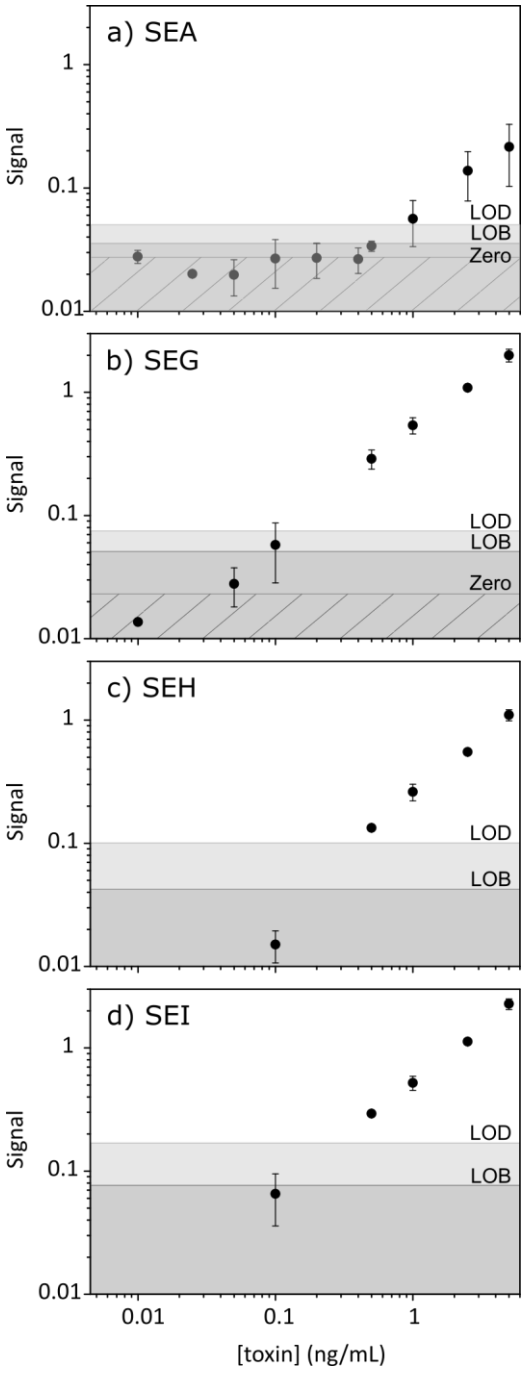

Figure S10: Quantitative analysis of range of SEA (a), SEG (b), SEH (c), and SEI (d) concentrations obtained in independent duplicates with gold NPs as probes (error bars indicate the standard deviation of two independent replicates). The zero, LOB and LOD are calculated from 8 independent replicates performed in the absence of toxin (zero = $mean_0$, LOB = $mean_0$ + 1.645 SD_0 and LOD = $mean_0$ + 3 SD_0, where the mean value of the test line signal in the absence of toxin is abbreviated $mean_0$ and its standard deviation SD_0).

S11 - Study of the potential cross-talk in view of multiplexing

All the "test line / toxin / Eu NPs" combinations are tested in simplex LFA labeled by Eu NPs. For instance, nanoparticles coated by SEI detection antibodies are used to detect the toxin SEH thanks to a strip designed to capture the toxin SEG. Experiments are carried out for a toxin concentration of 5 ng.mL^{-1}, that is the highest concentration used in this work for the non-multiplexed LFA. Images are quantitatively analyzed, the signal being defined as the ratio of the test line amplitude over the background. For the majority of the tested combinations, the signals are found to be lower than the LOBs determined in the standard configuration (e.g. SEH/SEH/SEH) with the same batch of strips (Table S11, left part, data in green). The only case of minor cross-talk appears when SEG capture antibodies are in the presence of the SEH toxin (Table S11, left part, data in red). Indeed, in the latter case, the non-specific signal represents 15 to 20 % of the signal obtained with the SEG/SEG/SEG system (Table S11, right part).

		Test / Background ([toxin] = 5 ng.mL^{-1})			Percentage of the signal in the standard (non-crossed) configuration		
		Eu NPs labelled by detection antibodies					
Capture antibody	Toxin	SEG	SEH	SEI	SEG	SEH	SEI
SEG	SEG	1.28	0.09	0.10	100.0	6.6	7.8
	SEH	0.27	0.19	0.21	20.7	14.9	16.1
	SEI	0.07	0.13	0.10	5.7	10.4	7.5
SEH	SEG	0.04	0.10	0.08	5.4	13.4	10.9
	SEH	0.02	0.71	0.04	2.7	100.0	5.9
	SEI	0.03	0.10	0.02	4.0	13.9	2.9
SEI	SEG	0.11	0.06	0.11	10.5	5.5	10.3
	SEH	0.09	0.07	0.01	8.7	7.0	0.8
	SEI	0.08	0.07	1.06	7.1	7.0	100.0

Table S11: Quantitative analysis of "test line / toxin / Eu Nps" combinations performed at 5 ng.mL^{-1} of toxin, the green and the red colours corresponding to signals being respectively lower and higher than the LOB (left part). The results are also displayed in percentages of the non-crossed combinations (right part).

Assuming that the percentage of cross-reactivity is independent of the toxin concentration, we can estimate the signal for all the "SEX/SEY/SEZ" combinations carried out for toxin concentrations of 0.5 ng.mL^{-1}. For this intermediate concentration, cross-talked signals are always found to be lower than the LOBs of the standard configuration. Even for the SEG test line and the SEH toxin combinations, the signal arising from cross-reactivity is 2 times lower than the LOB of the SEG/SEG/SEG configuration. Thus, the cross-reactivity at low toxin concentrations appears negligible, implying that there is no counter-indication for multiplexing LFA.

S12 – Quantitative analysis of multiplexed strips labeled with Eu nanoparticles

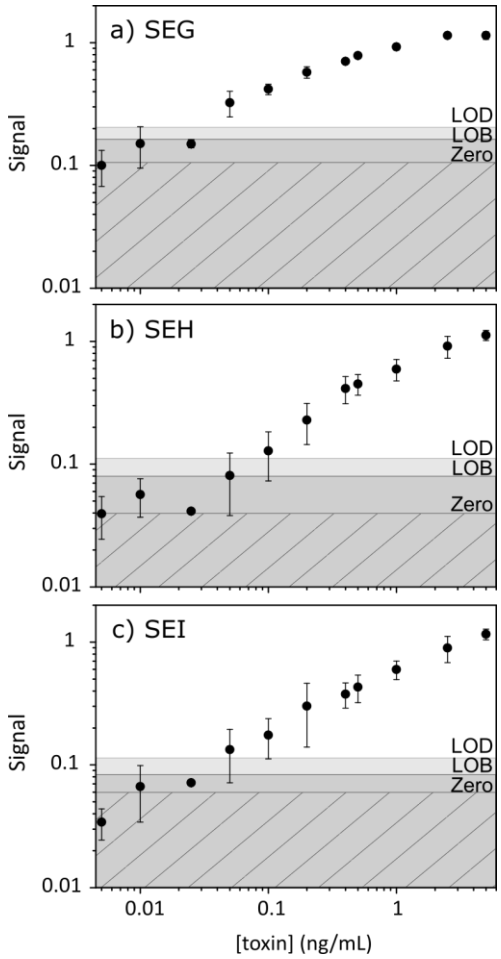

Figure S12: Quantitative analysis of SEG (a), SEH (b), and SEI (c) toxins performed in independent duplicates with Eu-doped NPs as probes for samples with identical SEG, SEH, and SEI concentrations. Error bars indicate the standard deviation of the two replicates. LOBs are determined at 0.02, 0.03, and 0.01 ng.mL^{-1} for SEG, SEH, and SEI respectively from 8 independent zeros.

[toxin] (ng/mL)	SEG	SEH	SEI
0	7.5	11.3	8.5
0.005	1.3	3.4	3.7
0.01	1.6	3.1	4.9
0.025	1.4	1.1	2.8
0.05	2.8	1.2	2.9
0.1	2.2	1.0	2.1
0.2	1.8	1.0	2.0
0.4	1.4	1.1	1.4
0.5	1.3	1.0	1.3
1	1.1	0.9	1.2
2.5	1.0	1.0	1.1
5	0.9	1.1	1.2

Table S12: Ratio between C_{exp} and C_{nom} where C_{exp} are the concentrations obtained from the experimental multiplexed signal via the calibration curves determined with the simplex assays and C_{nom} are the nominal concentrations of SEG, SEH, and SEI simultaneously spiked in samples. The values in grey boxes correspond to the ratio calculated for toxin concentrations below the LOBs. The ratios for all the other values are found respectively between 0.9-2.8, 0.9-1.2, and 1.1-2.9 for SEG, SEH, and SEI.

S13 – Multiplexed strips with different toxin concentrations

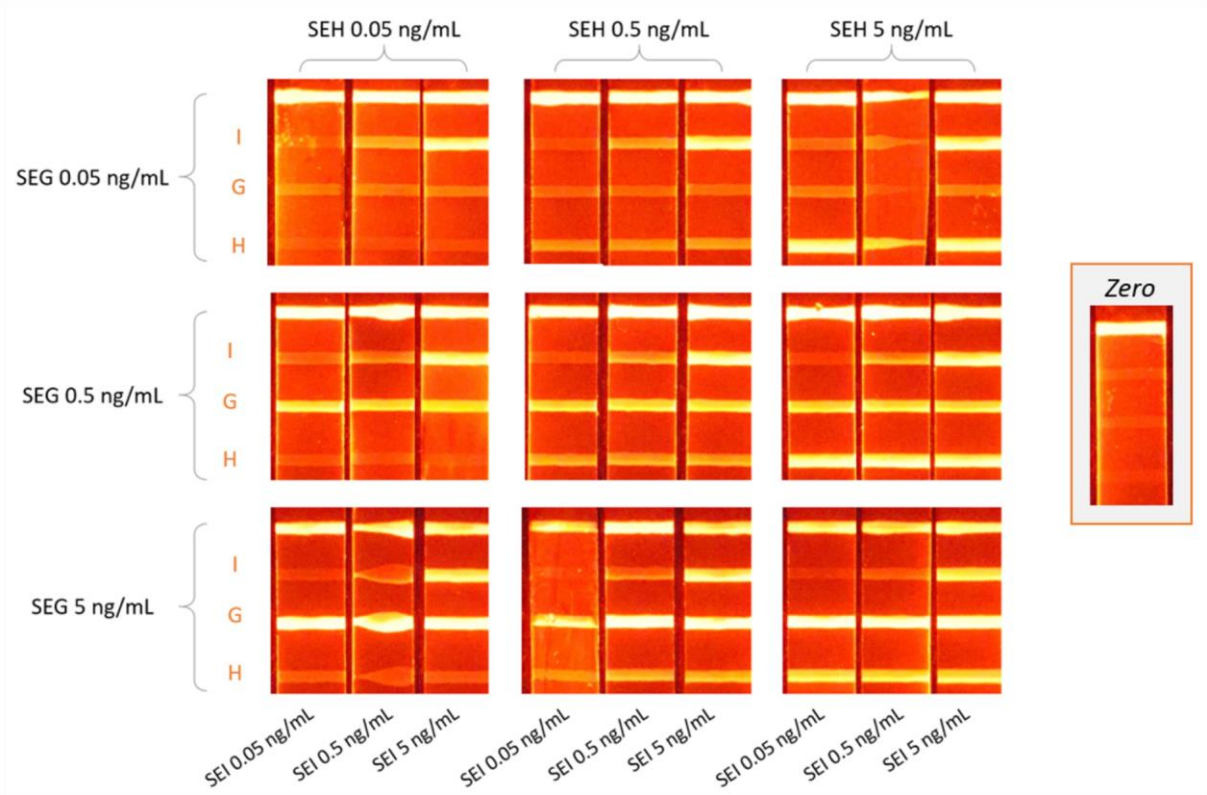

Figure S13: Combinatorial investigation of xLFA strips for SEG, SEH, and SEI concentrations at 0.05, 0.5, and 5 ng.mL^{-1}. Insert: "zero" strip, i.e. with no toxin present in the analysed sample.

References

1. Féraudet Tarisse, C. *et al.* Highly sensitive and specific detection of staphylococcal enterotoxins SEA, SEG, SEH and SEI by immunoassay. *Toxins* **13**, 130 (2021).
2. Huignard, A., Gacoin, T. & Boilot, J.-P. Synthesis and Luminescence Properties of Colloidal YVO_4:Eu Phosphors. *Chem. Mater.* **12**, 1090–1094 (2000).
3. Casanova, D. *et al.* Counting the Number of Proteins Coupled to Single Nanoparticles. *J. Am. Chem. Soc.* **129**, 12592–12593 (2007).
4. Giaume, D. *et al.* Organic Functionalization of Luminescent Oxide Nanoparticles toward Their Application As Biological Probes. *Langmuir* **24**, 11018–11026 (2008).
5. Haiss, W., Thanh, N. T. K., Aveyard, J. & Fernig, D. G. Determination of Size and Concentration of Gold Nanoparticles from UV−Vis Spectra. *Anal. Chem.* **79**, 4215–4221 (2007).
6. Kittel, C. Introduction to Solid State Physics. 12.
7. Fleury, B. *et al.* Amorphous to Crystal Conversion as a Mechanism Governing the Structure of Luminescent YVO_4:Eu Nanoparticles. *ACS Nano* **8**, 2602–2608 (2014).
8. Casanova, D. *et al.* Optical *in situ* size determination of single lanthanide-ion doped oxide nanoparticles. *Appl. Phys. Lett.* **89**, 253103 (2006).
9. Würth, C., Grabolle, M., Pauli, J., Spieles, M. & Resch-Genger, U. Comparison of Methods and Achievable Uncertainties for the Relative and Absolute Measurement of Photoluminescence Quantum Yields. *Anal. Chem.* **83**, 3431–3439 (2011).
10. de Puig, H., Bosch, I., Gehrke, L. & Hamad-Schifferli, K. Challenges of the Nano–Bio Interface in Lateral Flow and Dipstick Immunoassays. *Trends in Biotechnology* **35**, 1169–1180 (2017).